

Terahertz-induced interband tunneling of electrons in GaAs

W. Kuehn,¹ P. Gaal,^{1,*} K. Reimann,^{1,†} M. Woerner,¹ T. Elsaesser,¹ and R. Hey²

¹Max-Born-Institut für Nichtlineare Optik und Kurzzeitspektroskopie, 12489 Berlin, Germany

²Paul-Drude-Institut für Festkörperelektronik, 10117 Berlin, Germany

(Received 27 April 2010; revised manuscript received 24 June 2010; published 6 August 2010)

Ultrafast high-field transport is studied in *n*-type GaAs with ultrashort terahertz (THz) pulses of an electric field amplitude of up to 300 kV/cm. At lattice temperatures between $T=300$ and 80 K, we observe coherent ballistic transport of electrons over a major part of the first Brillouin zone. At $T=300$ K, ballistic transport occurs at a constant electron density whereas at lower temperatures, the THz pulses generate additional electron-hole pairs by field-induced tunneling between valence and conduction bands. We show that the ultrashort decoherence time of superpositions of valence- and conduction-band states plays a crucial role for the efficiency of the tunneling process. The extremely fast interband decoherence at room temperature results in a negligible tunneling rate.

DOI: 10.1103/PhysRevB.82.075204

PACS number(s): 78.47.jh, 72.20.Ht, 72.80.Ey

I. INTRODUCTION

In the periodic potential of a crystal, an electron under the action of an electric field performs a ballistic motion if scattering processes have a negligible influence. In this case, the change in electron wave vector \vec{k} with time is solely determined by the electric field acting on the electron,^{1,2}

$$\hbar \frac{d\vec{k}}{dt} = -e\vec{E}(t). \quad (1)$$

From the time-dependent wave vector, the momentary electron velocity is obtained via the gradient of the relevant band in the band structure (Fig. 1),

$$\vec{v}(\vec{k}) = \frac{1}{\hbar} \nabla_{\vec{k}} \mathcal{E}(\vec{k}). \quad (2)$$

Under most circumstances, the prerequisite for Eqs. (1) and (2), namely, that scattering is unimportant, is not fulfilled. If scattering is important, we typically find drift transport, described by the Drude model⁶ and concepts such as electron mobility.

Very recently,⁷ we have demonstrated that electrons in bulk *n*-type GaAs at room temperature ($T=300$ K) undergo coherent ballistic transport in the high electric field of several 100 kV/cm of short terahertz (THz) pulses. The THz field radiated by the accelerated electrons demonstrates that the carriers are coherently driven into the range of the conduction band where the effective mass becomes negative. A quantitative analysis shows that the coherent electron motion covers approximately half of the first Brillouin zone of bulk GaAs. Such results clearly demonstrate negligible friction due to incoherent scattering processes, in particular, polar optical-phonon scattering,^{8,9} on the few hundred femtosecond time scale of the experiments. The observed behavior is fully reproduced by quantum-kinetic transport calculations.

In this paper, we present an extension of the previous work⁷ toward lower lattice temperatures ($T=200$ K and $T=80$ K). The results presented in the following clearly demonstrate coherent carrier transport at such lower temperatures. In contrast to room temperature, the number of

electrons undergoing such motion is substantially enhanced and exceeds the number of electrons present by doping. This shows that the transient THz field promotes a substantial number of electrons from the valence into the conduction band, although the THz photon energy is much less than the band gap, $\hbar\omega_{\text{THz}} \ll E_g$. Field-induced tunneling from the valence to the conduction band represents the main mechanism enhancing the number of free carriers. The tunneling rate depends sensitively on the decoherence rate between valence- and conduction-band states. The temperature depen-

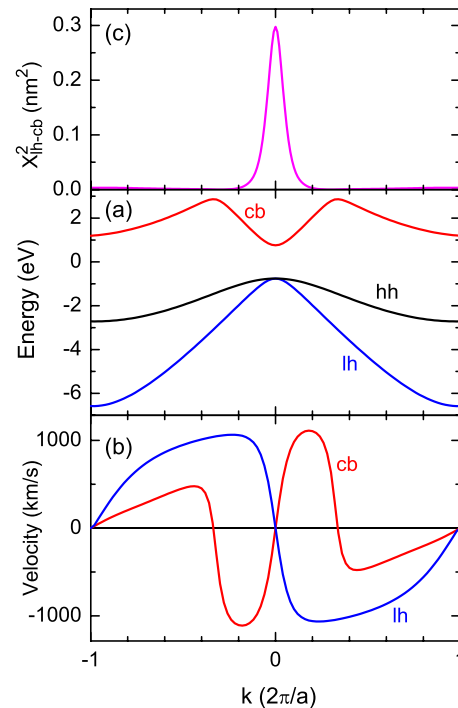


FIG. 1. (Color online) (a) Electronic band structure of GaAs along the [100] direction calculated by the local pseudopotential method without spin-orbit interaction (Refs. 3–5). (b) Corresponding velocity of electrons in the lowest conduction band (cb) and in the light-hole band (lh), Eq. (2). (c) Interband matrix element squared $X_{\text{lh-cb}}^2$ for the transition between the light-hole band and the lowest conduction band.

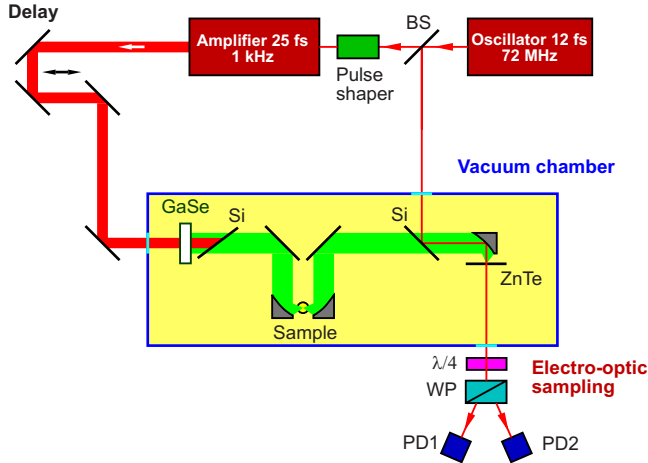


FIG. 2. (Color online) The Ti:sapphire oscillator-amplifier system generates 25 fs pulses at a wavelength of 800 nm with a repetition rate of 1 kHz and a pulse energy of 0.5 mJ. THz pulses, obtained by optical rectification in a GaSe crystal, are focused onto the sample, which is mounted on the cold finger of a cryostat. Electro-optic sampling in a [110] ZnTe crystal allows the measurement of the electric field as a function of delay time. The polarization state of the probe pulses from the oscillator is read out by the quarter-wave plate ($\lambda/4$), a Wollaston polarizer (WP), and the two photodiodes PD1 and PD2. The whole THz path and the sample are in a vacuum chamber.

dence of the decoherence rate leads to a temperature-dependent tunneling rate and, thus, to the experimentally observed difference between the results at room temperature and at lower temperatures.

II. EXPERIMENT

To study high-field transport on ultrafast time scales, we need both high electric driving fields and a method to determine the electron velocity as a function of time.

In our experiment (Fig. 2), high electric fields are applied to the sample in the form of strong THz pulses. The time dependence of the electric field acting on the sample is measured by electro-optic sampling.¹⁰⁻¹³ The same detection scheme is used to measure the electric field emitted by the electrons in the sample, which is in our geometry proportional to the current density j ,

$$j(t) = -en(t)v(t), \quad (3)$$

where $n(t)$ and $v(t)$ represent the time-dependent density and velocity of electrons.

The sample investigated was grown by molecular-beam epitaxy and consists of a 500 nm thin layer of n -type GaAs with a donor (Si) concentration of $N_D = 2 \times 10^{16} \text{ cm}^{-3}$ clad between two 300 nm thin $\text{Al}_{0.4}\text{Ga}_{0.6}\text{As}$ layers (the same sample was studied in Ref. 7). In the relevant area, the substrate is etched away¹⁴ so that the experiment is performed on a free-standing GaAs film.

THz pulses with a high electric field amplitude are generated by optical rectification of 800 nm pulses from a femtosecond Ti:sapphire oscillator-amplifier system. An acousto-

optic pulse shaper^{15,16} between oscillator and amplifier allows to tune both spectral amplitude and spectral phase to obtain a few-cycle THz pulse with a center frequency of 2 THz, which excites the sample placed in the focus of a pair of parabolic mirrors. The electric field of the transmitted THz pulse is measured via electro-optic sampling in a thin ZnTe crystal. The entire optical path of the THz beam is placed in vacuum.¹⁷⁻¹⁹ For the low-temperature measurements, the sample is mounted on the cold finger of a helium-flow cryostat, the latter being also placed in the vacuum chamber.

The electron current density,

$$j(t) = \frac{-2E_{\text{em}}(t)}{Z_0 d} \quad (4)$$

(see Appendix) in the sample is proportional to the coherently emitted field

$$E_{\text{em}}(t) = E_{\text{tr}}(t) - E_{\text{in}}(t), \quad (5)$$

which is given by the difference of $E_{\text{tr}}(t)$, the field transmitted through the sample, and $E_{\text{in}}(t)$, the field incident on the sample ($Z_0 = 377 \text{ } \Omega$, the impedance of free space). As the thickness of our sample $d = 500 \text{ nm}$ is much less than the THz wavelength $\lambda \approx 150 \text{ } \mu\text{m}$, all electrons in the sample experience the same driving field $E_{\text{loc}}(t)$, which is identical to $E_{\text{tr}}(t)$.^{18,20} The two transients $E_{\text{tr}}(t)$ and $E_{\text{in}}(t)$ are measured in separate scans, $E_{\text{tr}}(t)$ with the sample in place and $E_{\text{in}}(t)$ without the sample. Since the sample is very thin, the delay introduced by its refractive index has a very small value of 8 fs. This delay is taken care of when calculating $E_{\text{em}}(t)$, Eq. (5).

III. RESULTS

In Fig. 3, we show the incident and the emitted electric field transients measured at sample temperatures of 200 and 80 K for different amplitudes of the incident field. In all cases, one finds that in the beginning of the pulse $E_{\text{em}}(t)$ and $E_{\text{in}}(t)$ are out of phase, signifying absorption of the THz pulse in the sample. At later times, $E_{\text{em}}(t)$ and $E_{\text{in}}(t)$ are in phase, signifying THz emission.

Of particular interest is the comparison of the present low-temperature results with the results at room temperature, which have been discussed in detail in Ref. 7. At $T = 300 \text{ K}$, the amplitude of the emitted electric field is limited to about 7 kV/cm. The analysis in Ref. 7 shows that this amplitude agrees with the maximum emitted field possible for the electron density present by doping and the maximum electron velocity reached in ballistic transport (see Fig. 3 in Ref. 7). In contrast, at an incident amplitude of 300 kV/cm, the emitted field amplitude reaches 35 kV/cm at $T = 200 \text{ K}$ [Fig. 3(b)] and more than 50 kV/cm at $T = 80 \text{ K}$ [Fig. 3(d)]. In Fig. 4, we show $E_{\text{em}}(t)$ at $T = 80 \text{ K}$ for an incident amplitude of 300 kV/cm on an extended scale and compare it with the results at room temperature under otherwise identical conditions.

According to Eqs. (3) and (4), the emitted field is proportional to the electron density times electron velocity. The velocity is determined by the band structure [Eq. (2)], which

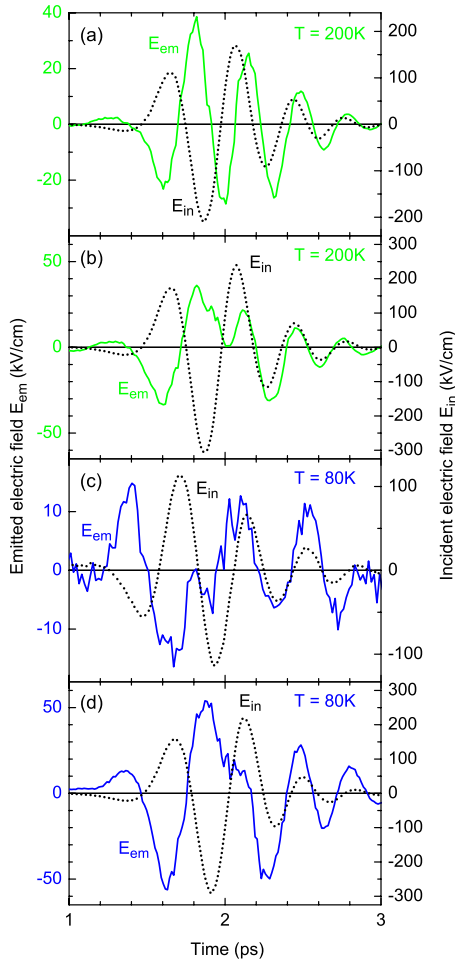


FIG. 3. (Color online) Transients of the incident [$E_{in}(t)$, dotted lines, right ordinate scale] and of the emitted [$E_{em}(t)$, solid lines, left ordinate scale] electric fields at temperatures of 200 K [(a) and (b)] and 80 K [(c) and (d)] for different field amplitudes.

changes only slightly as a function of lattice temperature. We thus conclude that the much higher amplitude of the field emitted at lower temperatures is due to an increase in the density of carriers contributing to the emission. Such an increase in electron density requires the promotion of electrons from the valence into the conduction band, i.e., an excitation energy equal to at least the band-gap energy $E_g = 1.5$ eV. To find out whether the THz pulse can provide the required energy density to the sample, we calculate the transiently absorbed energy¹⁸ normalized to the density N_D of electrons present by doping,

$$\begin{aligned} W_{abs}(t) &= \frac{1}{N_D} \int_{-\infty}^t j(t') E_{tr}(t') dt' \\ &= \frac{-2}{dN_D \mu_0 c} \int_{-\infty}^t E_{em}(t') E_{tr}(t') dt'. \end{aligned} \quad (6)$$

In Fig. 4(b), W_{abs} for $T=80$ K is plotted as a function of time (solid line). In the following, we consider two particular values of $W_{abs}(t)$, the maximum W_{max} and the value W_{irr} , the irreversibly absorbed energy after the end of the THz pulse.

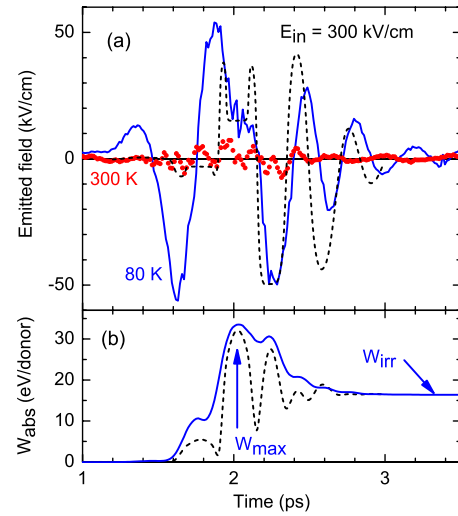


FIG. 4. (Color online) (a) Measured emitted field transients $E_{em}(t) = E_{tr}(t) - E_{in}(t)$ for lattice temperatures of $T=80$ K [solid line, same data as in Fig. 3(d)] and of 300 K (dots). Although the amplitude of $E_{in}(t)$ is 300 kV/cm in both cases, the low-temperature curve has an amplitude corresponding to a ten times higher carrier density, i.e., to $n_e \approx 10 \times N_D = 2 \times 10^{17}$ cm⁻³. (b) Normalized transiently absorbed energy [Eq. (6)] for $T=80$ K (solid line). After the THz pulse the absorbed energy of 15 eV corresponds to $\approx 2 \times 10^{17}$ cm⁻³ field-generated electron-hole pairs. The dashed lines in (a) and (b) are calculated from the theoretical model explained in Sec. IV.

During the THz pulse of an amplitude of 300 kV/cm, the sample at $T=80$ K stores a large amount of electromagnetic energy up to $W_{max} = 33$ eV. Part of this energy is reemitted, the remaining energy after the THz pulse of $W_{irr} = 17$ eV $\approx 10 \times E_g$ is the energy needed for the generation of $N = 10N_D = 2 \times 10^{17}$ cm⁻³ electron-hole pairs by the THz pulse. This number agrees well with the estimated density of nonlinearly emitting carriers contributing to the transient in Fig. 4(a).

In Fig. 5, we show W_{max} and W_{irr} as a function of incident field amplitude for temperatures between 80 and 300 K. The data at 300 K and the data at low amplitudes are taken from our previous work.^{7,17,18} Also shown is the range possible for W_{max} if no tunneling occurs, i.e., if the electron density stays equal to the doping density. In this case, the highest value for W_{max} is given by the highest energy an electron can have in the conduction band relative to the conduction-band minimum, that is 2.1 eV. The data for a temperature of 300 K stay within this range, showing that the electron density has not increased beyond the doping density. In contrast, for lower temperatures the data reach considerably higher values, signifying THz-induced tunneling from the valence into the conduction band. At an amplitude of 300 kV/cm and a temperature of 80 K, the energy per donor that is irreversibly absorbed reaches $W_{irr} = 17$ eV, sufficient for the generation of ten electron-hole pairs per donor.

IV. MECHANISM FOR THZ-INDUCED INTERBAND TRANSITIONS

There are two possible mechanisms for the transfer of electrons from the valence into the conduction band, impact

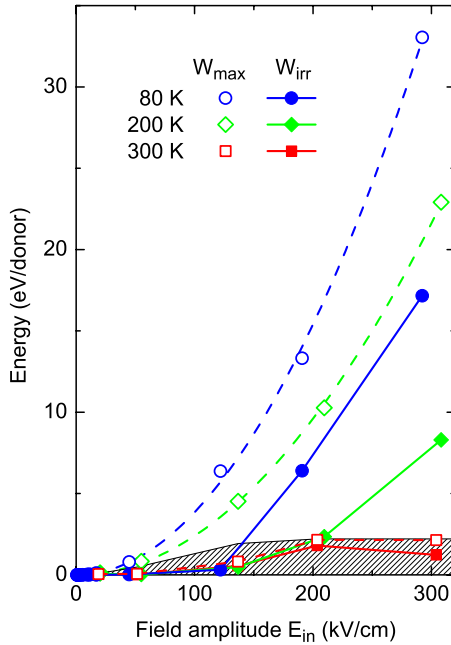


FIG. 5. (Color online) Maximum energy W_{\max} (open symbols) and irreversibly absorbed energy W_{irr} (closed symbols) as a function of the incident electric field amplitude, calculated according to Eq. (6), for temperatures of 80, 200, and 300 K. For $T=80$ K and for $T=200$ K, the dashed lines are fits to $W_{\max}=\text{const } E_{\text{in}}^2$. The hatched area shows the possible values for W_{\max} if only the electrons present by doping participate, i.e., if no tunneling occurs.

ionization and tunneling. An important issue for distinguishing between the two possibilities is whether the mechanism explains the experimentally observed temperature dependence, i.e., a negligible increase in electron density in the conduction band at room temperature and a strong increase at lower temperatures ($T=80$ and 200 K).

In impact ionization,^{21–29} an electron loses its kinetic energy to generate an electron-hole pair. This is only possible if the electron has a kinetic energy larger than the band gap.³⁰ Theoretical descriptions of impact ionization^{21,22} predict ionization rates that depend only on the electron kinetic energy and on the band structure. Thus, the lattice temperature influences the ionization rate only indirectly, either by changing the band structure or by preventing the electron to reach a sufficient kinetic energy. Both effects cannot explain our results. On the one hand, the band structure changes only little with temperature. On the other hand, our room-temperature results⁷ show that on our time scale temperature-dependent scattering processes do not influence the electron dynamics. Already at room temperature, we have ballistic transport. Thus, the kinetic energy the electrons reach is only determined by the electric field and by the band structure, which are both essentially temperature independent.

Another point that rules out impact ionization as an explanation for our results in GaAs is the low rate for impact ionization. The highest energy an electron can have in the lowest conduction band is 2.1 eV above the conduction-band minimum. For this kinetic energy, the impact ionization rate is 10^{12} s^{-1} , see Fig. 5 in Ref. 22. Thus, considering that the electron has such high kinetic energies only during a small

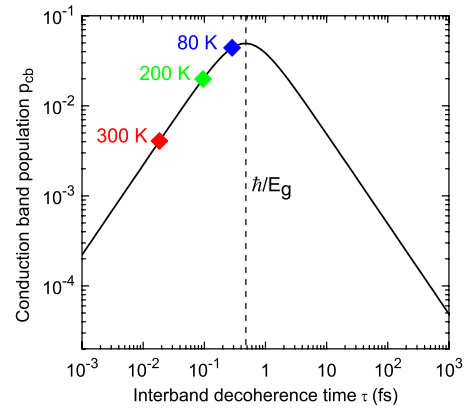


FIG. 6. (Color online) Population of the upper level (conduction band) after the end of the exciting THz pulse calculated for a two-level system as a function of the constant decoherence time τ (dots). The diamonds are estimates for the decoherence times at the temperatures of our experiment.

part of the pulse, impact ionization can at most account for the generation of 0.1 electron-hole pairs per initially present electron. Compared to the experimentally observed generation of ten electron-hole pairs this again shows that impact ionization is not able to explain our results.

Tunneling of electrons in high electric fields from the valence band into the conduction band is a well-known effect (Zener tunneling). Using the theoretical results for Zener tunneling in a static electric field,^{31–33} one finds a temperature-independent tunneling rate much lower than the rate needed to explain our results. For example, a tunneling rate close to zero is derived from Eq. (39) of Ref. 31 in a static electric field of 300 kV/cm. However, the model of Refs. 31–33 is not applicable to the present experiment as it neglects decoherence processes, i.e., the decay of quantum coherences between carrier wave functions of the initial and final states. As shown by Kazarinov and Suris^{34,35} (see also Ref. 36), decoherence strongly influences the tunneling rate R ,

$$R \propto \frac{\tau}{1 + (\Delta\omega\tau)^2}. \quad (7)$$

In this equation, the decoherence is described by the constant decoherence time τ (we shall see below that actually τ will not be constant), $\Delta\omega$ is the detuning from resonance of the initial and final state. For resonant tunneling ($\Delta\omega=0$) Eq. (7) shows that decoherence decreases the tunneling rate (the highest R is obtained for the longest τ). For nonresonant tunneling, however, the tunneling rate will increase up to the point where the decoherence time τ is equal to the inverse of the detuning $\Delta\omega$. For even shorter decoherence times, the tunneling rate decreases again [see Fig. 6].

In our case, the detuning is approximately E_g/\hbar , since the THz frequency is much smaller than the band gap. Thus, the highest tunneling rate is obtained for $\tau=0.5$ fs. Under the reasonable assumption that τ decreases with increasing temperature, the decoherence times at the temperatures of our experiment have to be near the values marked in Fig. 6 to explain our results.

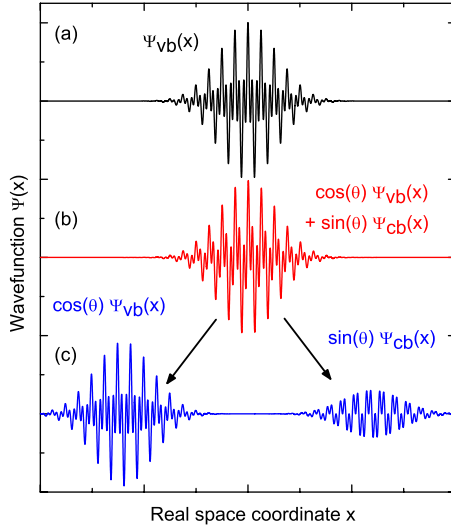


FIG. 7. (Color online) Dynamics of the electron wave function during interband tunneling: (a) valence-band electron wave packet (schematic) before THz excitation. (b) The THz field drives an off-resonant interband Rabi oscillation resulting in a coherent superposition of valence- and conduction-band wave packets. The amount of conduction-band character is determined by the parameter θ . (c) Further acceleration of the superposition will spatially separate the conduction-bandlike part from the valence-bandlike part of the same wave function with a pronounced nonclassical character.

At first sight, such short decoherence times seem unrealistic. Considering interband absorption, the sharpness of the observed features precludes decoherence times shorter than about 100 fs at room temperature and even longer at lower temperatures. However, the decoherence times for interband absorption and high-field THz transport are not the same. The decoherence time for high-field THz transport is much shorter than the decoherence time for interband absorption as explained in Fig. 7. An electron wave packet at the top of the valence band [part (a)] is exposed to a strong THz pulse. The electric field drives an off-resonant interband Rabi oscillation, i.e., it modifies the fast oscillating cell-periodic part of the wave function [part (b)], which results in a coherent superposition of a valence-band wave packet and a conduction-band wave packet. At the same time, the THz field drives an intraband motion of this coherent superposition. During this motion, the conduction-bandlike part moves in the opposite direction as the valence-bandlike part of the same wave function, resulting in an extremely “nonclassical” wave packet having two density maxima [part (c)]. In our experiment, the spatial separation of the two components can be as large as $\Delta x = 300$ nm. As shown by Zurek^{37–39} (see also Refs. 36, 40, and 41), such nonclassical wave packets experience high decoherence rates at finite temperatures T ,

$$\tau^{-1} = \tau_m^{-1} \frac{mk_B T (\Delta x)^2}{\hbar^2}. \quad (8)$$

In this equation, τ_m is the momentum relaxation time, responsible, e.g., for low-field transport. In contrast to the model used in Eq. (7) and for Fig. 6, the decoherence rate in Eq. (8) is not constant in time since it depends on the time-

dependent Δx . For a temperature of 80 K, one finds from the mobility $\tau_m = 1000$ fs. At the maximum Δx , this results in the very short decoherence time of 0.1 fs. Thus, Eq. (8) accounts (i) for the very short decoherence times needed for high tunneling rates and (ii) for the temperature dependence of decoherence (apart from the direct proportionality of the decoherence rate on T , $1/\tau_m$ increases with T). On the other hand, Eq. (8) still allows for sharp features in linear interband absorption since there Δx will be very small.

In contrast to the case considered in Refs. 34–36, Eq. (8) demonstrates a pronounced temperature dependence of τ . Taking this fact into account, we performed calculations considering on the same footing both interband and intraband transitions under the influence of an electric field. The electronic band structure was included in the form of a pseudopotential^{4,5} calculation neglecting spin-orbit interaction with a finite set of local pseudopotentials. The general Bloch wave function of an electron with wave vector \vec{k} in band b ,

$$\psi_{b,\vec{k}}(\vec{r}, t) = e^{i\vec{k}\vec{r}} \sum_{\vec{G}} c_{b,\vec{k},\vec{G}}(t) e^{i\vec{G}\vec{r}}, \quad (9)$$

is a coherent superposition of plane waves displaced by the reciprocal-lattice vectors \vec{G} . The coefficients $c_{b,\vec{k},\vec{G}}(t)$ are obtained from the following Hamiltonian, which includes the interaction with the external electric field via the vector potential $\vec{A}(t) = \int_0^t \vec{E}(t') dt'$ and the interaction with the periodic crystal potential:⁴²

$$[H^s(\vec{k}, \vec{A})]_{\vec{G}, \vec{G}'} = \frac{\delta_{\vec{G}, \vec{G}'}}{2m_0} [\hbar(\vec{k} + \vec{G}) - e\vec{A}]^2 + V(\vec{G} - \vec{G}'). \quad (10)$$

The $V(\vec{G})$ are the coefficients of the Fourier expansion of the periodic potential and m_0 is the free-electron mass. By diagonalizing the Hamiltonian H^s , one can transform it into the \vec{k} - and \vec{A} -dependent eigenbasis H^e , $H^e(\vec{k}, \vec{A}) = S(\vec{k}, \vec{A}) H^s(\vec{k}, \vec{A}) S^{-1}(\vec{k}, \vec{A})$. For $\vec{A} = 0$, the Hamiltonian yields the single-electron band structure, i.e., one gets the band energies $\mathcal{E}_b(\vec{k})$ and the corresponding coefficients $c_{b,\vec{k},\vec{G}}(t)$ for the band b .

In our calculations, we work in the single-particle picture, i.e., we neglect all many-body interactions, among them electron-electron scattering,⁴³ which could mix Bloch waves with different \vec{k} vectors. Without this mixing, each electron can be labeled by its initial \vec{k}_0 and band index b_0 before THz excitation. To include decoherence according to Eq. (8), we calculate the electron-hole distance as the time integral of the difference of the electron and hole velocities. The velocities in turn are obtained from the band structure [Eq. (2)]. For simplicity, we use a single decoherence rate for all electron-hole coherences, using the average electron-hole distance.

In the initial state of our system, all valence-band states are filled and all conduction-band states are empty.⁴⁴ The time evolution of the density matrix is obtained from the Liouville equation,

$$\frac{d\rho}{dt} = \frac{1}{i\hbar}[H(t),\rho] - \Gamma(t,\rho). \quad (11)$$

The last term in the equation above describes the decoherence. In principle, it is also necessary to consider spontaneous (incoherent) electron-hole recombination but this process can be neglected because of its low rate (typical lifetimes of electrons in the conduction band are in the nanosecond range). In solving Eq. (11), it is necessary to transform back and forth between the bases g and e mentioned above, using the transformation matrices S and S^{-1} . The first term in Eq. (11) is calculated in the basis g , the decoherence in the basis e . For the numerical calculation, the size of the time steps has to be below the shortest τ [Eq. (8)], i.e., at room temperature almost 0.01 fs, which makes the calculations very time consuming. From the calculation, one obtains the time dependence of the density matrix for the initial \vec{k} . The resulting current density is obtained as the expectation value of the velocity operator times the electronic charge and the emitted electric field from Eq. (4). The main results are: (i) tunneling can only occur at such points in k space where the interband matrix element $X_{b-b'}(\vec{k}) = \int \psi_{b,\vec{k}}^* X \psi_{b',\vec{k}} dV$ is high. The band-structure calculation allows the determination of these interband matrix elements. It turns out that they are zero for the transition from the heavy hole to the conduction band so that only tunneling from the light hole to the conduction band contributes. The square of this matrix element $X_{lh-cb}^2(\vec{k})$ is shown in Fig. 1(c). One finds the maximum of this matrix element and thus of the tunneling rate at the center of the Brillouin zone. It decreases for larger wave vectors so that only electrons with wave vectors within a diameter of 1/10 of the Brillouin zone can tunnel into the conduction band. From the corresponding k -space volume and the population probability, we obtain a total electron density of $3 \times 10^{17} \text{ cm}^{-3}$ in the conduction band, which agrees well with the observed value of $2 \times 10^{17} \text{ cm}^{-3}$.

For ballistic transport, the electron wave vector is proportional to the vector potential. Thus, one expects interband tunneling near the zeros of the vector potential. An additional requirement for interband tunneling is a high electric field. The effect of these two competing requirements is shown in Fig. 8(a). We see that the increase in the conduction band population is especially high if a high electric field and a zero of the vector potential A coincide (at $t=1.9 \text{ ps}$).⁴⁵ In contrast, for impact ionization the highest increase in the conduction-band population is expected near the extrema of the vector potential.

(ii) As mentioned already, decoherence plays an important role. Without decoherence, any tunneling is completely reversible [curve for $\gamma_m=0$ in Fig. 8(b)]. After the THz pulse, no electrons remain in the conduction band. For higher decoherence, we find an increasing conduction-band population after the end of the pulse, reaching 4×10^{-3} for $\gamma_m=(1 \text{ ps})^{-1}$, the value relevant for our experiment at low temperature. The corresponding population probability at room temperature is 5×10^{-4} , nearly a factor of 10 less.

(iii) Half of the additional current is carried by electrons in the conduction band, the other half by light holes. As can

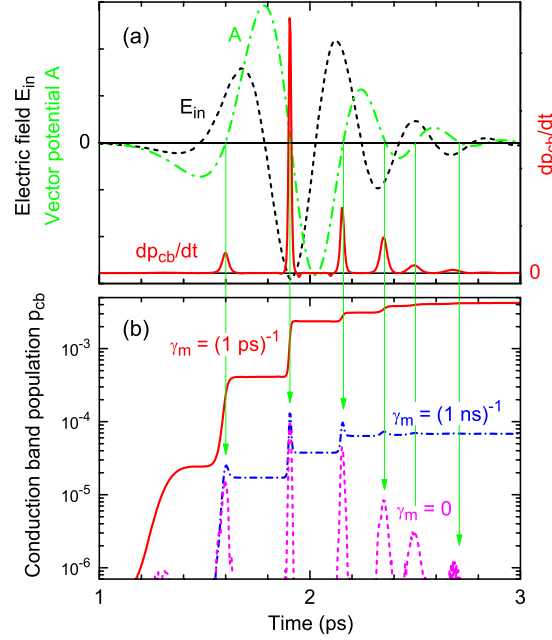


FIG. 8. (Color online) (a) Incident electric field $E_{in}(t)$ (field amplitude 300 kV/cm, dashed line), corresponding vector potential $A(t)$ (dashed-dotted line), and time derivative of the conduction-band population dp_{cb}/dt calculated for $\gamma_m=(1 \text{ ps})^{-1}$ and $T=80 \text{ K}$. The arrows mark the zeros of the vector potential. (b) Time dependence of the conduction-band population calculated for different momentum relaxation rates γ_m .

be seen in Fig. 1(b), the velocities in these bands are of comparable magnitude.

The theoretical curves in Fig. 4 (dashed lines) have been calculated with the model described above. While the time dependence of the absorbed energy $W_{abs}(t)$ agrees quite well with the theoretical curve [Fig. 4(b)], the calculated emitted electric field shows deviations, in particular in the beginning of the pulse [Fig. 4(a)]. Nevertheless, for such a simple model, which neglects all many-body effects such as electron-electron scattering and the formation of excitons, the agreement is satisfactory.

V. CONCLUSIONS

In conclusion, ultrafast high-field THz transients induce ballistic electron transport in bulk GaAs. At room temperature, it is possible for the electrons to traverse half the Brillouin zone for electric field amplitudes of 300 kV/cm.⁷ At lower temperatures (80 and 200 K), we observe additional THz-induced electron-hole pair generation, which leads to an increase in the density of free carriers by a factor of 10. The mechanism of this electron-hole pair generation is field-induced tunneling from the valence into the conduction band. The tunneling rate depends strongly on the decoherence of the coherent superposition of electron and hole states. Since the strong electric field accelerates electrons and holes in opposite directions, we get a highly nonclassical wave function, which decoheres very fast because of its coupling to the environment.

APPENDIX: MEASUREMENT OF VELOCITY VERSUS ACCELERATION OF ELECTRONS ON ULTRAFAST TIME SCALES

The electromagnetic field radiated by a single charged particle in motion is essentially proportional to its acceleration, see, e.g., Eq. (14.18) in Ref. 46. In our present experiment and in previous experiments,^{47–49} however, we do not deal with a single moving particle but rather an extended sheet of simultaneously moving particles. As a first approximation, we assume an infinite sheet of particles all moving with the same velocity. Because of interference between the individual contributions of all particles, it turns out that the electric field at the sample^{19,20,50} E_{sample} is proportional to the velocity of the moving charges or, equivalently, to the current density j in the sample (see Ref. 19 for a direct derivation using Maxwell's equations).

In the experiment, one does not directly measure E_{sample} but measures the electric field E_{det} at the electro-optic crystal. The relationship between E_{det} and E_{sample} depends on the optics used for the transfer of the electric field from the sample to the electro-optic crystal. We use a first parabolic mirror to collimate the radiation emitted from the sample and a second parabolic mirror to focus the radiation onto the electro-optic crystal [Fig. 9(a)]. Under the assumption of focusing mirrors collecting the entire solid angle, we get in this case $E_{\text{det}} = -E_{\text{sample}}$. Thus, the detected field is proportional to the electron velocity.

We now consider how deviations of the actual experimental conditions from the idealized assumptions influence the results. Using the formalism of Ref. 50, it is possible to calculate the electric field at the electro-optic crystal generated by a Gaussian current distribution on the sample. It turns out that the on-axis field ($\rho=0$) is proportional to the on-axis current density down to spot sizes of about one THz wavelength and, for the mirror sizes used (diameter 25.4 mm and parent focal length of 12.7 mm), in the frequency range ≥ 1 THz. This frequency range is perfectly adequate for our

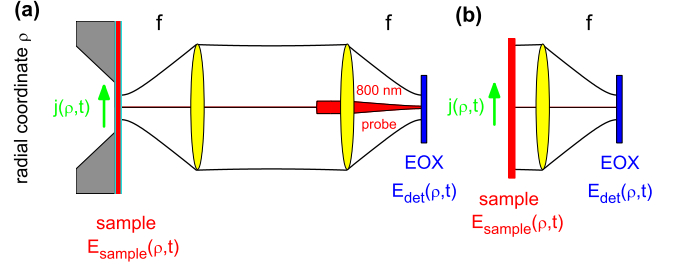


FIG. 9. (Color online) Two possible geometries for the transfer of the electric field from the sample to the electro-optic crystal (EOX). (a) In our setup, the radiation from the sample is collimated (in the actual experiment instead of lenses parabolic mirrors are used), propagates to the second lens and is focused onto the electro-optic crystal. This results in the on-axis ($\rho=0$) electric field at the detector $\vec{E}_{\text{det}}(0, t) = -\vec{E}_{\text{sample}}(0, t)$. Also shown is our sample with the etched substrate (gray). (b) In another often used setup (Refs. 47–49), the THz emission is focused by one lens onto the electro-optic crystal. This results in $\vec{E}_{\text{det}}(0, t) \propto \partial \vec{E}_{\text{sample}}(0, t) / \partial t$.

experiments since the incident field has negligible spectral density below 1 THz.

On the electro-optic crystal, the spot size of the probe beam is much smaller than the spot size of the THz beam. Therefore, we measure the on-axis THz field, as required by the analysis described. As a result, the signal measured in our setup is proportional to the electron *velocity*.

In contrast to our experiment, the setups of, e.g., Refs. 47–49 [Fig. 9(b)] use a single focusing element that images a large area of the sample onto a small spot on the electro-optic crystal. In the frequency domain, using Gaussian optics, one finds in this case $\vec{E}_{\text{det}}(\omega) \propto \omega \vec{E}_{\text{sample}}(\omega)$. The reason for this is that the size of the focal spot is proportional to the wavelength and thus inversely proportional to the frequency. In the time domain, this leads to $E_{\text{det}} \propto \partial E_{\text{sample}} / \partial t$. With $E_{\text{sample}} \propto v$ one thus gets in this case that the signal is proportional to the *acceleration* of the particles.

*Present address: Institut für Physik und Astronomie, Universität Potsdam, 14476 Potsdam, Germany.

†reimann@mbi-berlin.de

¹F. Bloch, *Z. Phys.* **52**, 555 (1929).

²B. K. Ridley, *Quantum Processes in Semiconductors*, 3rd ed. (Oxford University Press, Oxford, 1993).

³M. L. Cohen and T. K. Bergstresser, *Phys. Rev.* **141**, 789 (1966).

⁴J. R. Chelikowsky and M. L. Cohen, *Phys. Rev. Lett.* **32**, 674 (1974).

⁵J. R. Chelikowsky and M. L. Cohen, *Phys. Rev. B* **14**, 556 (1976); **30**, 4828(E) (1984).

⁶P. Drude, *Ann. Phys.* **306**, 566 (1900); **312**, 687(E) (1902).

⁷W. Kuehn, P. Gaal, K. Reimann, M. Woerner, T. Elsaesser, and R. Hey, *Phys. Rev. Lett.* **104**, 146602 (2010).

⁸G. E. Stillman, C. M. Wolfe, and J. O. Dimmock, *J. Phys. Chem. Solids* **31**, 1199 (1970).

⁹K. Fletcher and P. N. Butcher, *J. Phys. C* **5**, 212 (1972).

¹⁰Q. Wu and X.-C. Zhang, *Appl. Phys. Lett.* **67**, 3523 (1995).

¹¹Q. Wu, M. Litz, and X.-C. Zhang, *Appl. Phys. Lett.* **68**, 2924 (1996).

¹²Q. Wu and X.-C. Zhang, *Appl. Phys. Lett.* **71**, 1285 (1997).

¹³T. Bartel, P. Gaal, K. Reimann, M. Woerner, and T. Elsaesser, *Opt. Lett.* **30**, 2805 (2005).

¹⁴J. J. LePore, *J. Appl. Phys.* **51**, 6441 (1980).

¹⁵P. Tournois, *Opt. Commun.* **140**, 245 (1997).

¹⁶F. Verluise, V. Laude, Z. Cheng, C. Spielmann, and P. Tournois, *Opt. Lett.* **25**, 575 (2000).

¹⁷P. Gaal, K. Reimann, M. Woerner, T. Elsaesser, R. Hey, and K. H. Ploog, *Phys. Rev. Lett.* **96**, 187402 (2006).

¹⁸P. Gaal, W. Kuehn, K. Reimann, M. Woerner, T. Elsaesser, R. Hey, J. S. Lee, and U. Schade, *Phys. Rev. B* **77**, 235204 (2008).

¹⁹K. Reimann, *Rep. Prog. Phys.* **70**, 1597 (2007).

²⁰T. Stroucken, A. Knorr, P. Thomas, and S. W. Koch, *Phys. Rev. B* **53**, 2026 (1996).

- ²¹P. A. Wolff, *Phys. Rev.* **95**, 1415 (1954).
- ²²M. Stobbe, R. Redmer, and W. Schattke, *Phys. Rev. B* **49**, 4494 (1994).
- ²³I. Melngailis, G. E. Stillman, J. O. Dimmock, and C. M. Wolfe, *Phys. Rev. Lett.* **23**, 1111 (1969).
- ²⁴J. T. Devreese, R. G. van Welzenis, and R. P. Evrard, *Appl. Phys. A* **29**, 125 (1982).
- ²⁵S. Kolodinski, J. H. Werner, T. Wittchen, and H. J. Queisser, *Appl. Phys. Lett.* **63**, 2405 (1993).
- ²⁶S. D. Ganichev, J. Diener, and W. Prettl, *Appl. Phys. Lett.* **64**, 1977 (1994).
- ²⁷A. G. Markelz, N. G. Asmar, B. Brar, and E. G. Gwinn, *Appl. Phys. Lett.* **69**, 3975 (1996).
- ²⁸H. Wen, M. Wiczner, and A. M. Lindenberg, *Phys. Rev. B* **78**, 125203 (2008).
- ²⁹M. C. Hoffmann, J. Hebling, H. Y. Hwang, K.-L. Yeh, and K. A. Nelson, *Phys. Rev. B* **79**, 161201(R) (2009).
- ³⁰Because of momentum conservation, the generated hole will also have finite kinetic energy so that the threshold for impact ionization (2.1 eV according to Ref. 22) is even higher than the band gap.
- ³¹E. O. Kane, *J. Phys. Chem. Solids* **12**, 181 (1960).
- ³²J. V. Morgan and E. O. Kane, *Phys. Rev. Lett.* **3**, 466 (1959).
- ³³E. O. Kane, *J. Appl. Phys.* **32**, 83 (1961).
- ³⁴R. F. Kazarinov and R. A. Suris, *Fiz. Tekh. Poluprovodn.* **5**, 797 (1971) [*Sov. Phys. Semicond.* **5**, 707 (1971)].
- ³⁵R. F. Kazarinov and R. A. Suris, *Fiz. Tekh. Poluprovodn.* **6**, 148 (1972) [*Sov. Phys. Semicond.* **6**, 120 (1972)].
- ³⁶M. Woerner, K. Reimann, and T. Elsaesser, *J. Phys.: Condens. Matter* **16**, R25 (2004).
- ³⁷W. H. Zurek, *Phys. Today* **44**(10), 36 (1991).
- ³⁸W. H. Zurek, *Los Alamos Sci.* **27**, 86 (2002).
- ³⁹W. H. Zurek, *Rev. Mod. Phys.* **75**, 715 (2003).
- ⁴⁰A. O. Caldeira and A. J. Leggett, *Physica* **121A**, 587 (1983).
- ⁴¹A. J. Leggett, S. Chakravarty, A. T. Dorsey, M. P. A. Fisher, A. Garg, and W. Zwerger, *Rev. Mod. Phys.* **59**, 1 (1987).
- ⁴²M. Kira, W. Hoyer, and S. W. Koch, *Phys. Status Solidi B* **238**, 443 (2003).
- ⁴³The justification for neglecting electron-electron scattering in the calculation is that electron-electron scattering conserves total energy and total momentum of the electron system. Thus, the influence of electron-electron scattering is only indirect, leading to a redistribution within the electron system, which may in turn influence the dynamics. Furthermore, even at the highest electron density the typical electric field an electron generates at the position of another electron is only 5 kV/cm, much less than the applied electric fields.
- ⁴⁴Compared to the total number of conduction-band states, the number of electrons present because of doping is negligible.
- ⁴⁵For a bandwidth-limited pulse, the extrema of the electric field and the zeros of the vector potential always coincide but this is not the case for a pulse with chirp like in our experiment.
- ⁴⁶J. D. Jackson, *Classical Electrodynamics*, 3rd ed. (Wiley, Hoboken, 1999).
- ⁴⁷A. Leitenstorfer, S. Hunsche, J. Shah, M. C. Nuss, and W. H. Knox, *Phys. Rev. Lett.* **82**, 5140 (1999).
- ⁴⁸A. Leitenstorfer, S. Hunsche, J. Shah, M. C. Nuss, and W. H. Knox, *Phys. Rev. B* **61**, 16642 (2000).
- ⁴⁹M. Abe, S. Madhavi, Y. Shimada, Y. Otsuka, K. Hirakawa, and K. Tomizawa, *Appl. Phys. Lett.* **81**, 679 (2002).
- ⁵⁰L. W. Davis, *Phys. Rev. A* **19**, 1177 (1979).